Hindawi
International Journal of Polymer Science
Volume 2018, Article ID 7438694, 15 pages
https://doi.org/10.1155/2018/7438694

Research Article

Numerical Study on Seismic Behavior of Underwater Bridge Columns Strengthened with Prestressed Precast Concrete Panels and Fiber-Reinforced Polymer Reinforcements

Yu Tang,[1] Gang Wu,[1,2] and Zeyang Sun[1]

[1]*Key Laboratory of Concrete and Prestressed Concrete Structures of the Ministry of Education, Southeast University, Nanjing 210096, China*
[2]*Laboratory of Industrialized Structural and Bridge Engineering of Jiangsu Province, Nanjing 210096, China*

Correspondence should be addressed to Gang Wu; g.wu@seu.edu.cn and Zeyang Sun; sunzeyang@seu.edu.cn

Received 26 March 2018; Revised 3 July 2018; Accepted 15 July 2018; Published 7 August 2018

Academic Editor: Filippo Berto

The seismic performance of the bridge column, such as pier or pile, is a time-dependent property which may decrease in resistance to the deterioration or natural hazards along the structure's service life. The most effective strengthened method for degraded bridge columns is the jacketing method, which has been widely developed and investigated through numerous studies since the 1980s. This paper presented a modeling method, as well as a comprehensive parametric study, on seismic performance of bridge columns strengthened by a newly developed strengthening method with prestressed precast concrete panels and fiber-reinforced polymer reinforcements (PPCP-FRP). A modeling method of bridge columns strengthened with PPCP-FRP was first presented and validated with test results. The influence of design parameters, such as axial load ratio, equivalent FRP reinforcement ratio rate (EQFRR), expansion ratio, and shear span ratio of strengthened columns, were then further evaluated in terms of lateral load capacity, ductility, energy dissipation, lateral stiffness, and residual displacement of strengthened columns. The peak load of strengthened columns increases with the increasing of EQFRR due to the unique failure model of strengthened columns characterized by the fracture of FRP bars. The initial stiffness of strengthened columns increased by 300% with the increasing of expansion ratio by 45%, and a stable postyield stiffness stage was obtained by most strengthened columns in analysis. The residual displacement of strengthened columns decreases rapidly with the increasing of EQFRR, which indicated that a better repairability could be achieved by the strengthened column with a relatively high EQFRR.

1. Introduction

The seismic performance degradation objectively exists on underwater bridge columns, as piers and piles, during their long-term service periods due to unpredictable factors, such as extreme scouring or corrosion, which have been identified as the most common causes of bridge failures in the United States [1, 2]. The most effective retrofitting method for the degraded bridge columns is jacking; their forms, as well as their seismic effects, have been widely developed and investigated through numerous experimental studies since the 1980s.

Concrete jacketing was the earliest developed method used to enhance the lateral stiffness and strength of the columns. Priestley et al. [3] reported that adding a relatively thick layer of reinforced concrete (RC) in the form of a jacket around the column could enhance the flexural strength and shear strength of columns. Bett et al. [4] reported a repairing study with concrete jacket subject to a shear deficient RC column, showing that the columns strengthened by concrete jacket became much stiffer and stronger laterally than the original column. Meanwhile, the drawbacks of concrete jacketing were also obvious such as high cost, low efficiency, and limited effect on flexural strength and ductility

improvement; therefore, steel jacketing was developed in the 1990s. Chai et al. [5] reported a retrofitting investigation on a circular column, which was designed with an insufficient lap splice length of the longitudinal bars, with a bonded steel jacket at its plastic hinge region, and showed that steel jacket retrofitting could effectively restore the flexural strength and ductility of the column and improve the lateral stiffness by 10 to 15 percent. Studies on failure mode investigation conducted by Priestley et al. [6] proved that steel jacket retrofitting could also change the inelastic deformation pattern of the columns, from the predominantly shear deformation for the as-built columns to the predominately flexural deformation for the retrofitted columns, and the elastic stiffness and ductility of the columns could also be significantly improved simultaneously.

From the 21st century, new materials and methods have been developed to keep up with the gradually increasing demand for retrofitting, such as high durability and low vulnerability, in which the development and use of FRP composites could be the most representative example in structural retrofitting projects. One of the most attractive applications of FRP composites is their use as confining devices for concrete columns, which may result in remarkable increases in strength and ductility [7, 8]. It is proved by many researches that the FRP composites, especially with high deformability and low elastic modulus, such as basalt fiber composites [9], polyethylene terephthalate (PET) fiber-reinforced polymer composites [8, 10], and FRP ropes [11, 12], have a positive effect to the axial compressive ability of FRP-confined concrete. The FRP composites could also be used as the longitudinal reinforcement to improve the seismic performance of bridge columns such as flexural capacity, yet have little impact on, or might even lower, the lateral stiffness of the strengthened columns, especially when the FPR bars were embedded into the columns [13–16]. Other researchers concentrated on the combination of the different jacketing methods. The prestressed steel jacketing (PSJ) was developed by Fakharifar et al. [17] for rapid and cost-effective repair of severely damaged circular RC columns. The results showed that the PSJ successfully restored the ultimate stress and displacement ductility of the columns, but only limitedly restored the initial stiffness of the column by 84% of the as-built column. Meanwhile, the anchored dowel bar showed its essential role in resisting lateral force; by linking the column and footing with anchored dowel bars, the lateral performance of the column such as ultimate stress, initial stiffness, and displacement ductility were all enhanced by at least 20%. Li et al. [18] also reported an experimental investigation on the corrosion-damaged RC columns strengthened with a combined CFRP sheet and steel jacket, which indicated a better effectiveness than the columns strengthened with only CFRP sheets or steel jacket in terms of strength and ductility. Conventional jacketing methods could enhance the flexural strength, shear strength, or even ductility of columns but with unneglectable drawbacks, such as high cost, low efficiency, and poor durability. With the recognition of life-cycle maintenance requirement and the advancement of retrofitting methods for the structures, new efficient jacketing methods were demanded to keep up with the gradually increased demand on retrofitting, such as high durability and low vulnerability.

This paper presented a modeling method, as well as a comprehensive parametric study, on seismic performance of bridge columns strengthened by a newly developed strengthening method with PPCP-FRP. The PPCP-FRP method is mainly developed for the rapid retrofitting of the underwater bridge columns, for which conventional retrofitting usually requires a cofferdam construction ahead of the repairing to build a relatively easy-to-work construction environment, which is a far less ideal one due to its low cost-efficiency and applicability. The PPCP-FRP method enhanced the cost-efficiency and applicability by using the prestressed precast concrete panel (PPCP) as the formwork (cofferdam). A modeling method of bridge columns strengthened with PPCP-FRP was first presented and validated with test results. The influence of design parameters, such as axial load ratio, EQFRR, expansion ratio, elastic modulus of FRP reinforcement, compressive strength of concrete, and shear span ratio of column, were then further evaluated in terms of the lateral load capacity, ductility, energy dissipation, lateral stiffness, and residual displacement of strengthened columns.

2. Modeling Method of Bridge Columns Strengthened with PPCP-FRP Method

2.1. Design of PPCP-FRP Method. The PPCP-FRP retrofitting is mainly composed of precast concrete panels, steel strands, longitudinal FRP bars, FRP spiral stirrup, and mortar, as in Figure 1(a). The principle of strengthening with reinforced concrete is adopted in PPCP-FRP retrofitting to achieve a significant improvement on the lateral stiffness of the column; however, to enlarge the section of the column, instead of using a common steel mold, a newly developed quick-assembled concrete mold, composed of precast concrete panels (PCP), is applied to facilitate the construction process. The longitudinal FRP bars, which are embedded into the column base, as well as the FRP spiral stirrup were adopted as the strengthening reinforcement to enhance the overall flexural capacity and repairability of the column. Prestressed steel strands were used to integrate PCPs into a fixed ring; however, due to the fact that prestressing was relatively low (less than 10% of the ultimate tensile strength of steel strands), its confinement effect (to concrete materials) was mostly neglected in this paper considering the stress lagging. The mortar was used for filling up the space between the original column and PCP to join the original column, FRP reinforcement, and PCP together. The retrofitting processes could be summarized as follows: (a) embedding of FRP bars into the column base, (b) installation of the FRP spiral stirrup, (c) assembly of PCP, (d) prestress steel strands, and (e) grouting, as shown in Figure 1(b). The detailing of embedding FRP bars into the column base was shown in Figure 1(c), and an embedding depth of 350 mm was applied for all kinds of FRP bars in this paper.

2.2. Modeling. The modeling of bridge columns strengthened with the PPCP-FRP method was based on the fiber analysis

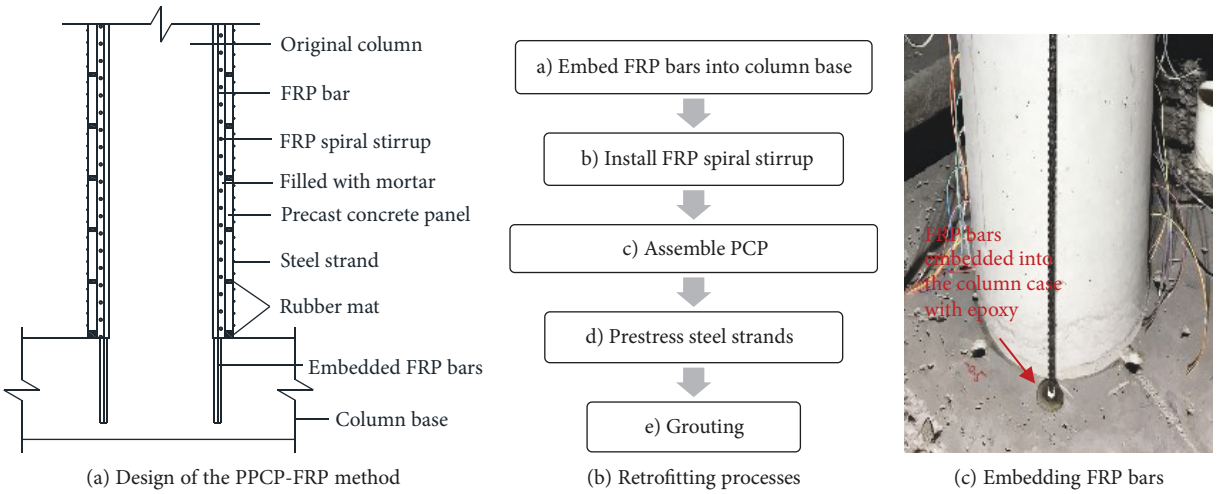

(a) Design of the PPCP-FRP method (b) Retrofitting processes (c) Embedding FRP bars

Figure 1: Design and retrofitting processes of the PPCP-FRP method.

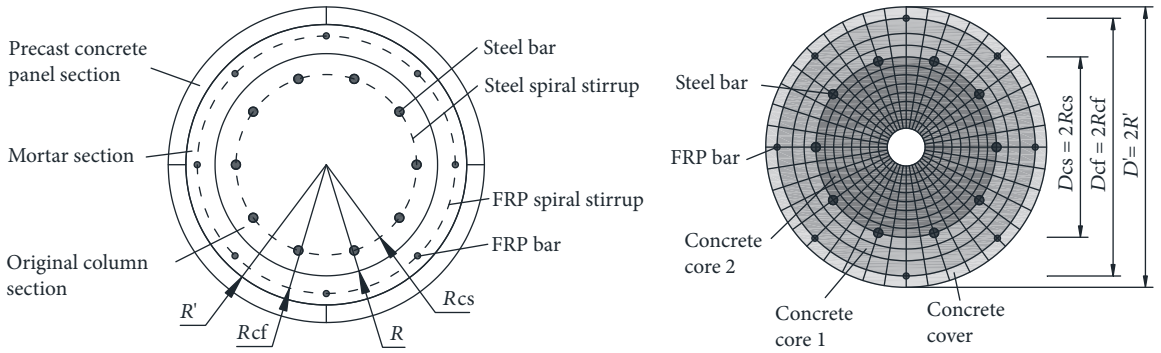

(a) Cross section in experiment (b) Cross section in OS

Figure 2: Cross section of the strengthened column.

concept, in which the flexural member was represented by unidirectional material fibers, and was realized in OpenSees (OS) [19].

The real cross section and the modeling cross section of strengthened specimens are shown in Figure 2. The real cross section is composed of the PCP section, the mortar section, and the original column section, as shown in Figure 2(a). The PCP section was excluded from the modeling cross section due to its minor contribution on vertical load bearing and transverse confinement to the column. The mortar and original column sections were divided into three sections in modeling, which were concrete core 1, concrete core 2, and concrete cover, as shown in Figure 2(b), based on the different confinement conditions applied by steel spiral stirrup and FRP spiral stirrup. Particularly, the cover of the original column and the mortar confined by the FRP spiral stirrup were considered with only one section (concrete core 1) in modeling, which was based on the fact that the concrete cover of the original column usually had deteriorated and would be removed anyway before the retrofitting, as in the experiment.

The real column in the experiment and the column model in the modeling are shown in Figure 3. In the experiment, three 1/4-scale circular-section bridge columns were initially designed and manufactured. The diameter and height of the initial column were 300 mm and 1275 mm, respectively, and the shear span ratio equaled to 4.25, a little larger than those in other common columns, which was to ensure that the shear span ratios of the specimens would be larger than 3 after strengthening; therefore, the flexure failure mode could be achieved. The volumetric transverse reinforcement ratio was equal to 0.09%. One of the columns was regarded as the control column, while the other two were further strengthened with PPCP-FRP, as shown in Figure 3(a). Different types of FRP reinforcement, which are referred to as basalt fiber-reinforced polymer (BFRP) reinforcement and carbon fiber-reinforced polymer (CFRP) reinforcement, were used as strengthening reinforcements for different specimens; however, the strengthening reinforcement ratio, calculated based on the equivalent strength principle, remained almost the same for both specimens, as shown in Table 1, in which ρ_{orl} refers to the longitudinal reinforcement ratio of the original column (i.e., control column) before strengthening, as in (1); n_s refers to the amount of longitudinal steel bars; A_s refers to the cross-sectional area of longitudinal steel bars; A_{cr} refers to the

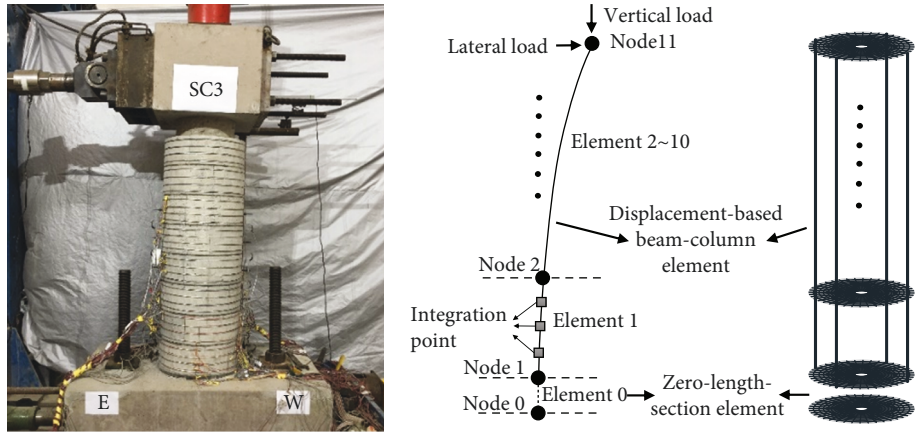

(a) Real column under testing (b) Column model in OS

Figure 3: Real column and column model.

Table 1: Details of all the specimens.

Specimen label	ρ_{orl} (%)	Strengthening reinforcement			ρ_{eql} (%)
		Type	FRP bar/ρ_{eqfl} (%)	FRP spiral stirrup/ρ_{eqft} (%)	
CC	1.1	\	\	\	1.1
SCB	1.1	BFRP	8Φ7.8/1.1	Φ5.9@50/1.8	1.8
SCC	1.1	CFRP	8Φ6/1.2	Φ4@40/1.9	1.9

cross-sectional area of the original column; ρ_{eqfl} and ρ_{eqft} refer to the additional equivalent longitudinal and transverse reinforcement ratio of strengthened columns, respectively, as in (2) and (3); n_f refers to the amount of longitudinal FRP bars; $A_{cr}{}'$ and $d_{cr}{}'$ refer to the cross-sectional area and diameter of the strengthened columns, respectively; $d_{cr}{}'$ equals to 370 mm in this paper; s refers to the spacing of the FRP spiral stirrup; A_{eqfl} and A_{eqft} refer to the equivalent longitudinal and transverse cross-section areas of the FRP bars, which were calculated based on the equivalent strength princeple, as shown in (4) and (5); f_{ufl} and f_{uft} refer to the ultimate stress of longidufinal and transverse FRP bars, respectively; A_{fl} and A_{ft} refer to the actual cross-sectional areas of longitudinal and transverse FRP bars, respectively; and ρ_{eql} refers to the equivalent longitudinal reinforcement ratio of the strengthened column, as in (6).

$$\rho_{orl} = \frac{n_s \cdot A_s}{A_{cr}}, \tag{1}$$

$$\rho_{eqfl} = \frac{n_f \cdot A_{eqfl}}{A_{cr}{}'}, \tag{2}$$

$$\rho_{eqft} = \frac{4A_{eqft}}{s \cdot d_{cr}{}'}, \tag{3}$$

$$A_{eqfl} = \frac{f_{ufl}A_{fl}}{f_s}, \tag{4}$$

$$A_{eqft} = \frac{f_{uft}A_{ft}}{f_s}, \tag{5}$$

$$\rho_{eql} = \frac{n_f A_{eqfl} + n_s A_s}{A_{cr}{}'}. \tag{6}$$

The tests were performed using a loading system, as shown in Figure 3(a). All of the specimens were subjected to a combination of constant axial load and lateral cyclic loads. A constant axial load of 287 kN (normalized axial load ratio equals to 0.16) was first applied to each specimen with a hydraulic jack. Then, the lateral cyclic load was first controlled by a force which started at ±10 kN and then increased by ±10 kN at each load step until the column yielded. After the column yielded, the cyclic loading pattern was converted to a displacement-based control and each load step was repeated three times. Each specimen was instrumented with the following devices to measure its lateral load and corresponding displacement, deformations, and strains: (1) load sensor installed at the head of the actuator, (2) LVDT installed on the top of the specimen that works with the load sensor to measure displacement, and (3) strain gauges bonded onto the reinforcing bars.

A column model, which is composed of displacement-based beam-column (DBBC) elements (element 1 ~ 10) and zero-length-section element (element 0), was built in modeling, as shown in Figure 3(b). Each DBBC element contained three integration points. The zero-length-section element was located at the bottom of the model to consider the strain penetration of longitudinal bars. Node 0 was fully fixed during the test, while node 1 was constrained only at dof 1 and 2. In addition, the vertical and lateral loads were applied to node 11 and the loading patterns were exactly the same as in the experiment.

2.3. Material Parameters. Two different kinds of concrete were used to build the original column and PCP, respectively. The 28-day compressive strengths ($f_c{}'$) of these concretes were equal to 25.1 MPa and 40.5 MPa, respectively, and the corresponding elastic moduli (E_o) were equal to 24.9 GPa and 36.3 GPa. The 28-day compressive strength

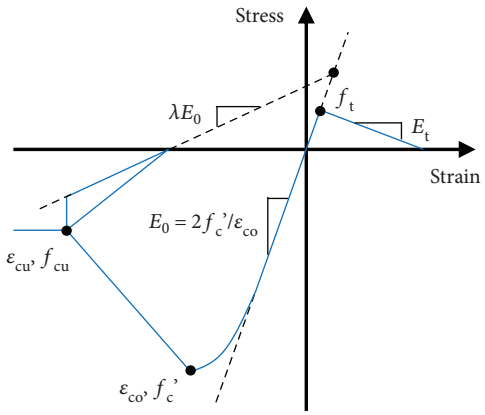

Figure 4: Model of concrete in OS.

and elastic moduli of mortar were equal to 32.7 MPa and 22.6 GPa, respectively.

Concrete 02 in OS was used for simulating the concrete material, which was realized by defining the initial elastic tangent (E_o), compressive strength (f_c'), compressive strain ($\varepsilon_{co} = 4f_c'/E_o$), ultimate strength (or crushing strength for unconfined concrete) (f_{cu}), ultimate strain (or crushing strain for unconfined concrete) (ε_{cu}), tensile strength (f_t), and ratio (λ) between unloading slopes at ε_{cu} and E_o, as shown in Figure 4. The modified Kent-Park model [20] was used as the compressive skeleton curve, which maintained a balance between simplicity and accuracy. For unconfined concrete, the crushing strength was usually set to "0" (or a quiet small value), which represents that no strength was considered for unconfined concrete after it was crushed. However, for concrete cover in this paper, the crushing strength should be considered due to the fact that the outside PCPs kept in a good shape until the end of the experiment, which means that a relatively strong confinement could be continuously applied to the "concrete cover" even after it has crashed. Due to a lack of experimental studies on axial compressive behavior of concrete confined with PCPs, 0.5 times of compressive strength was assumed for the crushing strength of concrete cover, and the crushing strain equals to −0.004. For concrete core 1 and concrete core 2, the ultimate strengths and strains would be enhanced by the single or dual confinements provided by the FRP spiral stirrup and steel spiral stirrup. However, due to a lack of experimental studies, a series of existing FRP-confined concrete models [21–23] were adopted to calculate the ultimate strengths and strains for the concrete materials. For concrete core 1, the ultimate strength and strain were calculated by using the FRP sheet confined concrete model proposed by Wu et al. [21]; the ultimate strength was taken as 1.8 times of its compressive strength, and the ultimate strain equals to −0.02. For concrete core 2, the ultimate strength and strain were expected to be larger than those of concrete core 1 due to an extra confinement provided by the steel spiral stirrup [22]. However, due to the potential negative effects such as stress lagging of the FRP spiral stirrup or a weak old-new concrete interface, which could possibly lower the ultimate strength, a conservative ultimate strength, which equals to 2 times of the compressive strength [23], was taken for concrete core 2, and the corresponding crushing strain remains the same with that of concrete core 1. The detailed setting of the parameters of concrete materials in OS are shown in Table 2.

The dimensions and mechanical properties of all reinforcements used in the experiment were experimentally measured, as listed in Table 3, in which D and E refer to the diameter and elastic modulus of reinforcement, respectively, f_y and f_u refer to the yield stress and ultimate stress of reinforcement, respectively, and ε_u refers to the fracture strain of reinforcement.

Steel 02 material in OS was adopted for modeling the longitudinal steel bars in modeling, by defining parameters such as elastic modulus of steel bar (E_s), yield stress, strain-hardening ratio ($b = 0.01$) between postyield tangent and initial elastic modulus, and transition parameters from elastic to plastic branches ($R_0 = 18$, $cR_1 = 0.9$, and $cR_2 = 0.15$) [19]. *Hysteretic material* in OS was applied for modeling the longitudinal FRP bars by defining stress and strain values of feature points on the envelope curve [19]. The compressive strength of FRP bars was assumed equal to 50% of its tensile strength, and the compressive elastic modulus was assumed the same as the tensile elastic modulus based on the experimental studies conducted by Deitz et al. [24]

2.4. Comparison between Test Results and Modeling Results. In the experiment, a classic flexural failure mode including concrete crushing and longitudinal steel bar buckling (some fractured in the end) was observed for the CC specimen, as shown in Figure 5(a). The test phenomena of SCB and SCC were basically the same. After the test, the concrete panels of SCB and SCC were removed and the fracture of longitudinal FRP bar was observed, as in Figure 5(b).

The hysteresis load-displacement (L-D) curves of all specimens showed that the overall seismic performances of all strengthened specimens, including the lateral loading capacity, stiffness, and ductility, were significantly enhanced through the strengthening process with PPCP-FRP, as shown in Figure 6. Due to the relatively big ultimate strain of BFRP reinforcements, the force level of BFPR reinforcements in SCB would be smaller than that of CFPR reinforcements in SCC when similar strains were applied to these FRP reinforcements, as illustrated in (7), in which F_f refers to the force level of the FPR reinforcement, E_f refers to the elastic modulus of the FRP reinforcement, and A_f and A_{eqf} refer to the actual and equivalent cross-section area of the FPR reinforcement. This could be further illustrated as follows: The increasing speed of the force level would be relatively slow for the FRP reinforcement with a relatively high ultimate strain in the strengthened column, which could be beneficial to the adequate utilization of the material strength (especially to the steel reinforcement in original column) and therefore enhance the stability and energy dissipation capacity of the strengthened column.

$$F_f = \varepsilon E_f A_f = \varepsilon f_s A_{eqf} \frac{E_f}{f_u} = \varepsilon f_s A_{eqf} \cdot \frac{1}{\varepsilon_u}. \quad (7)$$

Table 2: Detailed setting of the parameters of concrete materials in OS.

Concrete material parameters	Setting value in OS		
	Concrete core 2	Concrete core 1	Concrete cover
f_c' compressive strength	−25.1 MPa	−32.7 MPa	−32.7 MPa
E_o elastic modulus	24.9 GPa	22.6 GPa	22.6 GPa
ε_{co} compressive strain	$4 * f_c'/E_o$	$4 * f_c'/E_o$	$4 * f_c'/E_o$
f_{cu}/f_c' ratio of ultimate strength (or crushing strength) to compressive strength	2.0	1.78	0.5
ε_{cu} ultimate strain (or crushing strength)	−0.02	−0.02	−0.004
f_t tensile strength	$-0.14 * f_c'$	$-0.14 * f_c'$	$-0.14 * f_c'$
E_t tension softening stiffness	$f_t/0.002$	$f_t/0.002$	$f_t/0.002$
λ ratio of unloading slope at ε_{cu} to E_o	0.1	0.1	0.1

Table 3: Dimensions and mechanical properties of all reinforcements.

Reinforcement type	D/mm	E/GPa	f_y/MPa	f_u/MPa	ε_u/%
Steel bar	10	210	446	615	16.8
Steel spiral stirrup	6	210	446	615	16.8
Steel strand	3	161	\	1653	2.4
BFRP bar	7.8	63	\	1382	2.2
BFRP bar/BFRP spiral stirrup	5.9	63	\	1382	2.2
CFRP bar	6	170	\	2560	1.5
CFRP spiral stirrup	4	170	\	2560	1.5

The L-D curves of all specimens were consistent with the experimental curves, as shown in Figure 6. The hysteretic curves of all specimens agreed well with those in experiments. The characteristic values of L-D curves, as shown in Figure 7, as well as their errors with the characteristic values of experimental curves, were calculated and are listed in Table 4. The yield load (F_y) and peak load (F_p), as well as their corresponding displacements (Δ_y, Δ_p), agreed well with the test results with the maximal errors of 3.6% and 12.1%, respectively. In addition, the postyield stiffness of the L-D curves was calculated, as shown in Table 4, which also agreed well with those of test results with a maximal error of 11.1%. Moreover, the residual displacement of the L-D curves, which equals to the mean value of the positive and negative residual displacements of the L-D curve of each cycle, was compared with that of experimental curves in Figure 8, in which the residual displacement values were basically consistent with the experimental residual displacement values especially within the residual displacement limit, which was 1% of the column height according to the Japanese code [25], as shown in Figure 8(a). Furthermore, the development of residual displacement with the drift ratio of L-D curves agreed well with those of experimental curves, as shown in Figure 8(b), all of which indicated a high accuracy of the modeling method on predicting the seismic behavior of columns strengthened by the PPCP-FRP method.

3. Parametric Study

3.1. Parameter Setting. A comprehensive parametric study was conducted to further evaluate the seismic performance of the strengthened columns with different parameters, such as axial load ratio (n), EQFRR (α_ρ), expansion ratio (κ_s), elastic modulus of FRP reinforcement (E_f), compressive strength of concrete ($f_{co}{}'$), and shear span ratio of the column (λ). The set value of each parameter, corresponding to the contrivable range for each parameter, are listed in Table 5.

The axial load ratio in this paper particularly equals to the axial load divided by the compressive strength of concrete and the cross-sectional area of the original column. A common range of axial load ratio for bridge columns, which was 0.05 ~ 0.2, was adopted.

The EQFRR equals to the ratio of the additional equivalent longitudinal reinforcement ratio of the strengthened column to the longitudinal reinforcement ratio of the original column, as in (8), and a range of 0.05 ~ 0.43 was adopted for EQFRR.

$$\alpha_\rho = \frac{\rho_{\text{eqfl}}}{\rho_{\text{orl}}}. \tag{8}$$

The expansion ratio equals to the ratio of D_{cf} to D_{cs}, as shown in Figures 2(b) and (9). It should be noted that two major factors were coupled in κ_s, which were the expansion of the cross-section area and the variation of the distribution of FRP bars, considering the irrationality of the strengthening design by simply enlarging the cross-sectional area without rearranging the FRP bars. In this paper, the thickness of the concrete cover was fixed at 20 mm for all possible set values of the expansion ratio, which means that when a bigger κ_s was applied in the analysis, a farther distance would be achieved by FRP bars away from the neutral axis of the cross section.

$$\kappa_s = \frac{D_{\text{cf}}}{D_{\text{cs}}}. \tag{9}$$

The elastic modulus of FRP reinforcement was designed for considering the different types of FRP reinforcements manufactured with different fibers, such as glass fiber, aramid fiber, basalt fiber, and carbon fiber. The ultimate

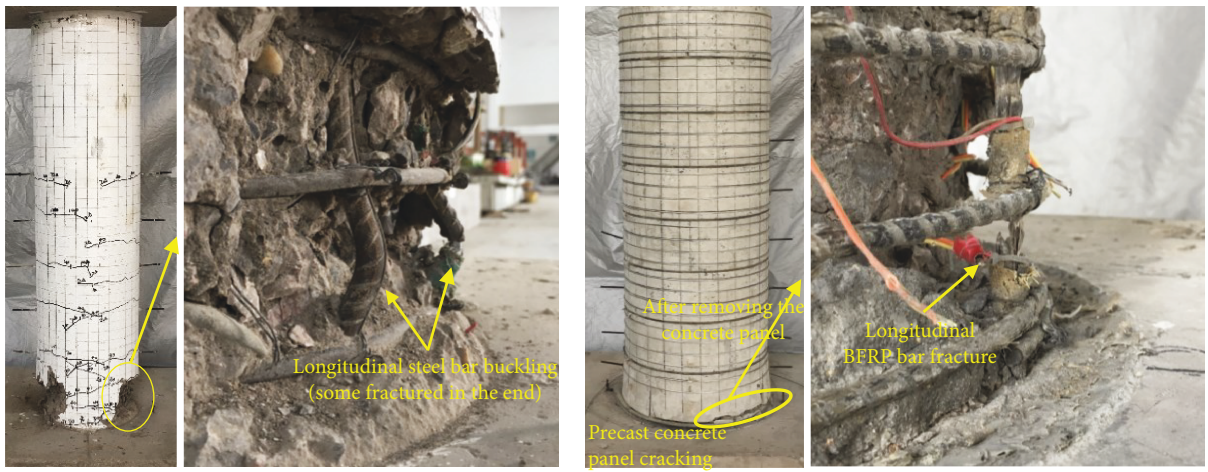

(a) CC (b) SCB

Figure 5: Failure mode of the specimens.

strength of these FRP reinforcements usually differs from each other but within a certain range. In this paper, a conservative value (1400 MPa) for the ultimate strength of FRP reinforcements was set for all kinds of FRP reinforcement to simplify the modeling approach. Therefore, the ultimate strain of FRP reinforcement would vary with E_f due to the inverse relationship between these two factors; basically, when a bigger E_f was applied, a smaller ultimate strain would be achieved by FRP reinforcement in the parametric study.

The compressive strength of the concrete and the shear span ratio of the column were also considered in a parametric study according to the design and analysis basics for the bridge column [3, 26]. The shear span ratio equals to the column height divided by the cross-sectional diameter of the original column.

A default value for each parameter was proposed, as in Table 5, for conducting the qualitative study on seismic behavior of strengthened columns. When a specific parameter was being investigated, other parameters could fix at the default value and would not impose any effect to the results.

3.2. Typical Load-Drift Curves with the Variation of Specific Parameter

3.2.1. Axial Load Ratio. The typical load-drift curves with the variation of axial load ratio are shown in Figure 9(a), in which the yield load and peak load of the curves increase with the increase in axial load ratio. The increase in yield load was due to the fact that the yield of steel bars was postponed because of the relatively slow development of stress in steel bars when a relatively high axial load ratio was applied. In addition, increasing the axial load ratio would potentially increase the flexural bearing capacity of the column by increasing the depth of the compression zone of the cross section of the column, in which case the peak force of the column would be enhanced, as displayed on the typical load-drift curves.

3.2.2. EQFRR. The typical load-drift curves with the variation of EQFRR are shown in Figure 9(b), in which the postyield stiffness, peak force, and corresponding drift ratio increase with the increase in EQFRR. A relatively high postyield stiffness could be expected for the specimens with a relatively large EQFRR due to the fact that a relatively high lateral load would be achieved by a strengthened column during the postyield stiffness stage when a relatively large EQFRR was applied under a certain drift ratio. In addition, since the cross-section failure of the column was characterized by the fracture of FRP bars in analysis, the peak moment of the cross section would increase, while the depth of the compression zone of the cross section would decrease with the increase in EQFRR; therefore, the peak force and corresponding drift ratio would increase with the increase in EQFRR.

3.2.3. Expansion Ratio. The typical load-drift curves with the variation of expansion ratio are shown in Figure 9(c), in which the initial stiffness, postyield stiffness, and peak force increase, while the drift ratio of the peak force decreases with the increase in expansion ratio. Since the lateral stiffness of the circular column was proportional to the fourth power of the cross-sectional diameter, a significant enhancement of initial stiffness and postyield stiffness should be expected by simply increasing the expansion ratio. In addition, enlarging the cross-sectional area of the column fundamentally equals to a decrease in shear span ratio of the column and reduction in the depth of the compression zone of the cross section, which would further lead to an increase in peak force and a decrease in its corresponding drift ratio.

3.2.4. Elastic Modulus of FRP Reinforcement. The typical load-drift curves with the variation of elastic modulus of FRP reinforcement are shown in Figure 9(d), in which the postyield stiffness increases, while the drift ratio of the peak force decreases with the increase in elastic modulus of FRP reinforcement. The increase in the postyield stiffness was due to the same reason as in EQFRR. The decrease in drift ratio of the peak force was due to the fact that a relatively high

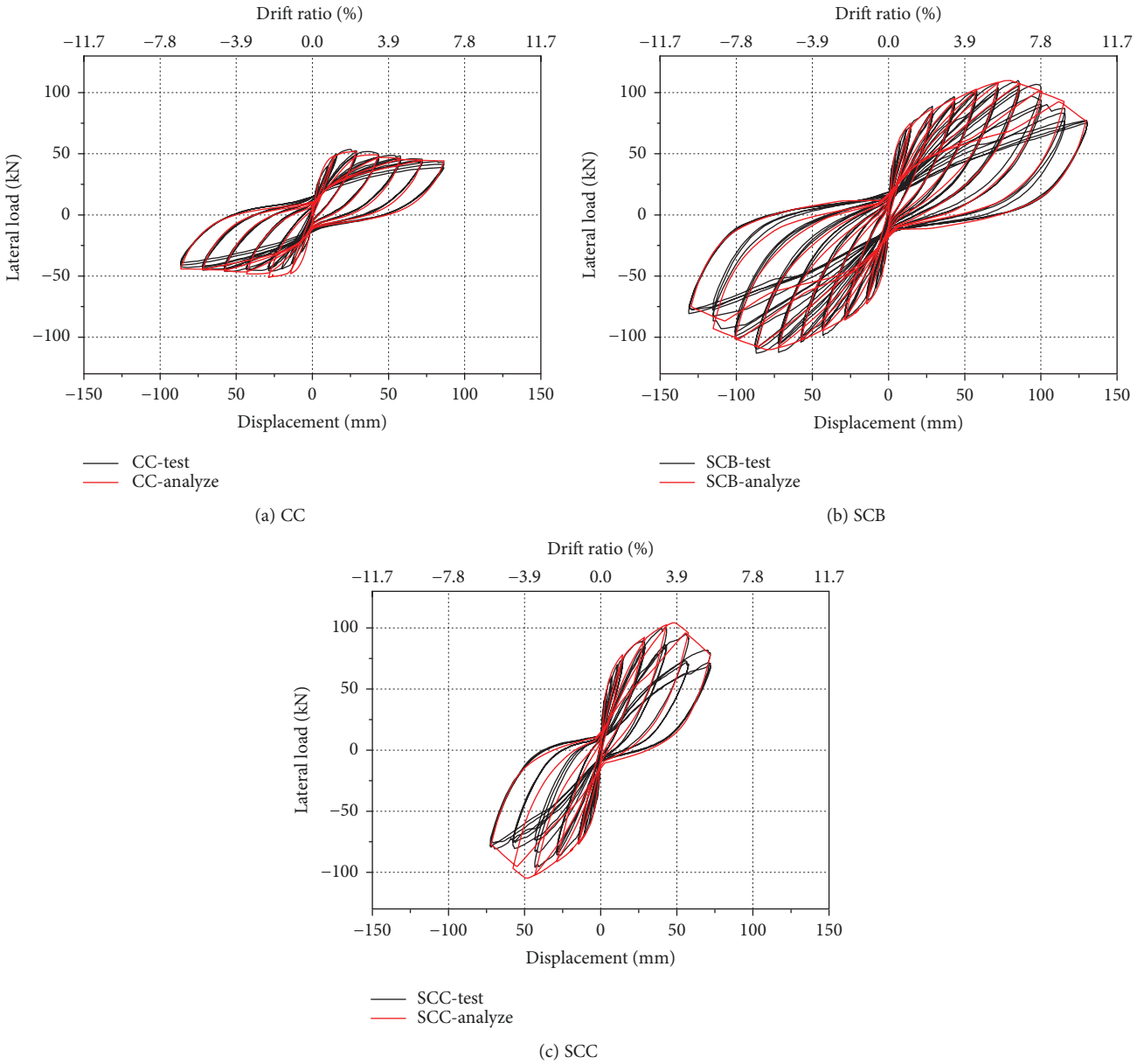

Figure 6: L-D hysteresis curves of all specimens.

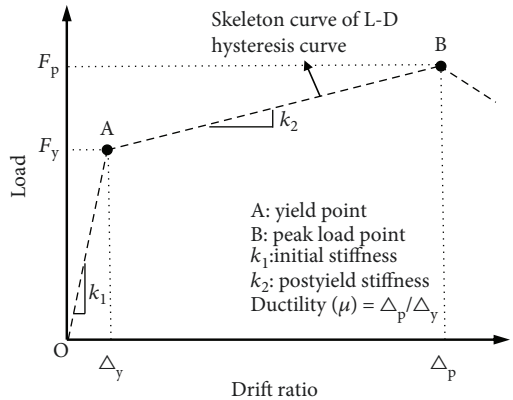

Figure 7: Schematic diagram of characteristic values of L-D hysteresis curves.

elastic modulus implied a relatively low ultimate strain for FRP reinforcement when the ultimate strength of FRP reinforcement was fixed in a parametric study.

3.2.5. Compressive Strength of Concrete and Shear Span Ratio of Column. The typical load-drift curves with the variation of the compressive strength of concrete are shown in Figure 9(e), in which the drift ratio of the peak force decreases with the increase in compressive strength of the concrete, which was due to the indirect effect imposed by the decrease in depth of the compression zone of the cross section. The typical load-drift curves with the variation of the shear span ratio of the column are shown in Figure 9(f). Since the effect of the shear span ratio of the column was basically overlapped within the effect of the expansion ratio, a similar tendency was displayed on these two sets of curves.

Table 4: The characteristic values of calculated L-D hysteresis curves and the error to the test results.

Specimen label	F_y		Δ_y		F_p		Δ_p		k_2	
	Analysis (kN)	Error (%)	Analysis (mm)	Error (%)	Analysis (kN)	Error (%)	Analysis (mm)	Error (%)	Analysis (mm)	Error (%)
CC	47.3	2.1	12.9	10.4	51.97	3.0	27.6	12.2	\	\
SCB	74.53	1.0	14	9.1	109.8	0.1	78.8	8.8	0.54	11.1
SCC	74.2	2.9	11.9	4.0	104.1	3.6	47.3	12.1	0.84	11.1

Error = |test − analyse|/test.

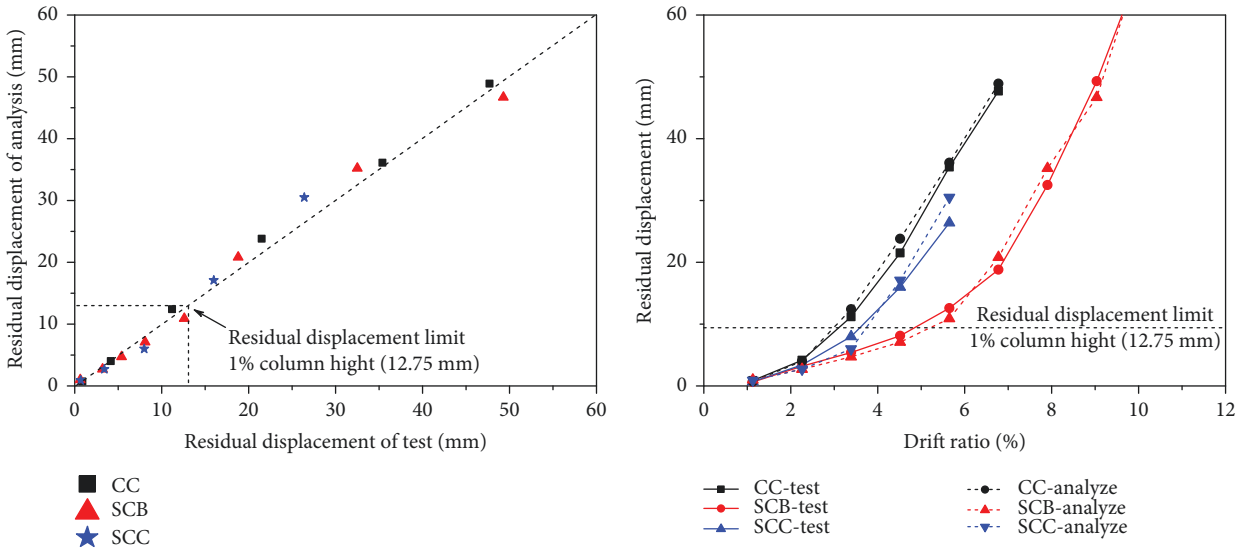

(a) Residual displacement value

(b) Drift ratio-residual displacement curve

Figure 8: Comparison between modeling and test results on residual displacement.

Table 5: Parameter value setting.

Parameters	n	α_ρ	κ_s	E_f/GPa	f_{co}'/MPa	λ
Set value	0.05	0.05	1.1	25	15	3.5
	0.1	0.11	1.2	50	25	4.5
	0.15	0.18	1.4	100	35	5.5
	0.2	0.25	1.6	150	45	6.5
		0.33		200		
		0.43				
Default value	0.1	0.11	1.4	50	25	4.5

The increase in initial stiffness and postyield stiffness, with the decrease in shear span ratio, was due to the fact that the lateral stiffness of the circular column was inversely proportional to the square of the column height. The increase in peak force and the decrease in corresponding drift ratio, with the decrease in shear span ratio, were basically due to the same reason as analyzed in the expansion ratio.

3.3. Effect of the Parameters to the Seismic Performance

3.3.1. Lateral Load Capacity and Ductility. The yield load and peak load are two representative characteristics of the lateral load capacity of the column. Among all parameters, EQFRR showed the most significant effect on yield load and peak load. When the steel bars of the column began to yield, a relatively high stress would be achieved by FRP bars when a relatively high EQFRR was applied, and the yield load of the column would increase with the increase in EQFRR. In addition, since column failure was characterized by the fracture of FRP bars, when a higher EQFRR was applied for strengthened columns, a higher peak load would be obtained. As shown in Figure 10(a), the peak load of specimens significantly increased with the increase in EQFRR. Moreover, the shear span ratio affects the yield load and peak load of the column as well, by presenting an approximate inverse relationship with both yield load and peak load, due to the same reason as common RC columns [27].

The ductility (μ) of the column, as in Figure 7, is mostly influenced by EQFRR and elastic modulus of FRP reinforcement, as shown in Figure 11. The ductility decreases with the increase in EQFRR, as shown in Figure 11(a), due to the fact that the yield of the column had been postponed with the increase in EQFRR; the reason is presented in Figure 10(a). The ductility decrease with the increase in elastic modulus of FRP reinforcement, as shown in Figure 11(b), was simply due to the fact that the drift ratio of the peak load had significantly decreased with the increase in elastic modulus of FRP reinforcement; the reason is illustrated in Figure 9(d).

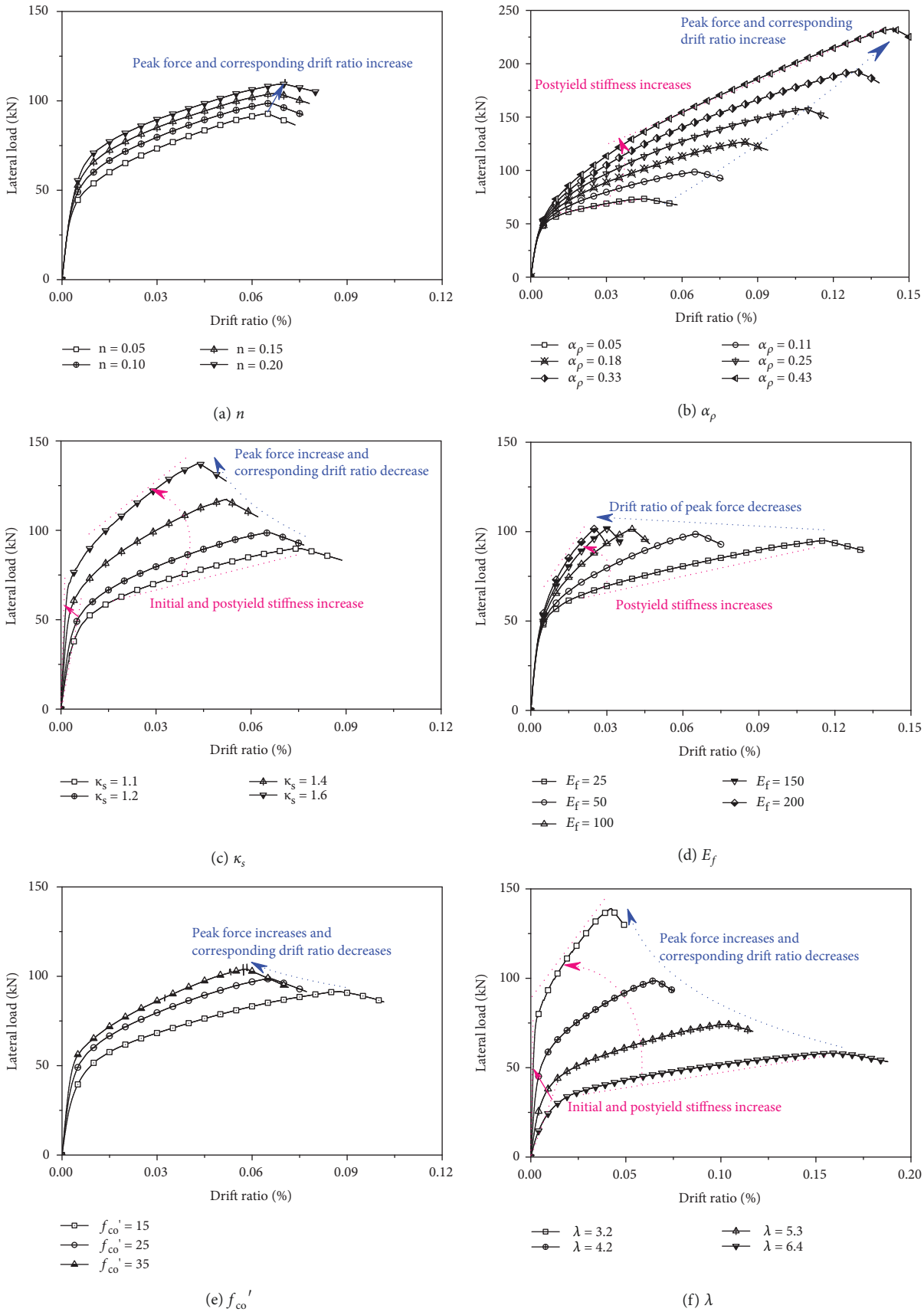

Figure 9: Typical load-drift curves with the variation of different parameters.

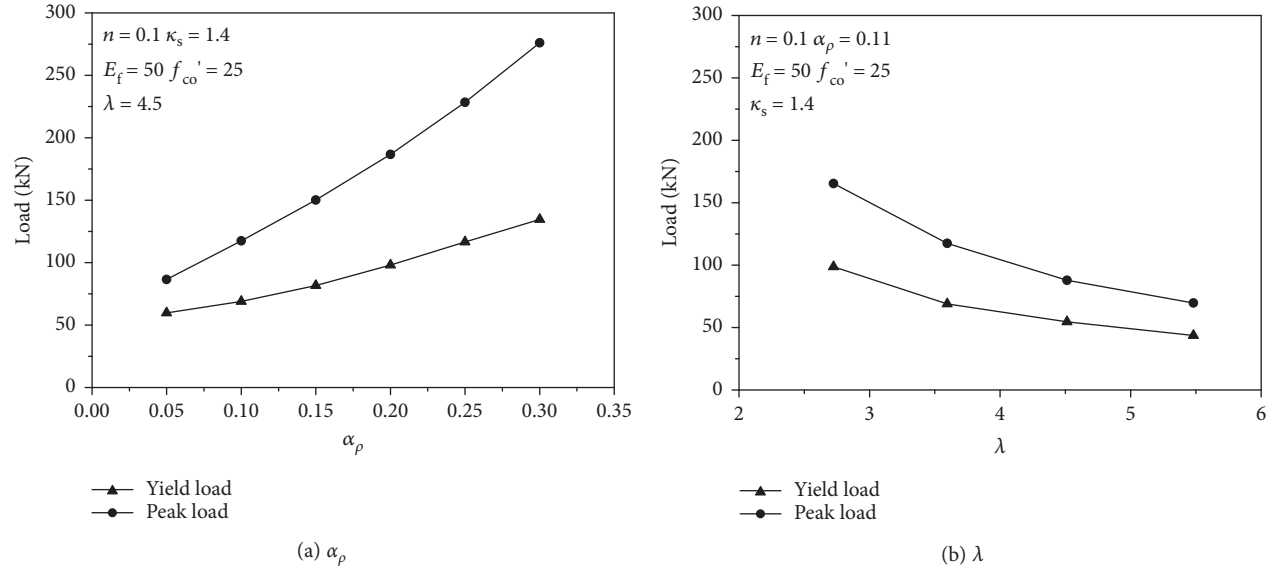

(a) α_ρ (b) λ

Figure 10: Variation of the characteristic load with different parameters.

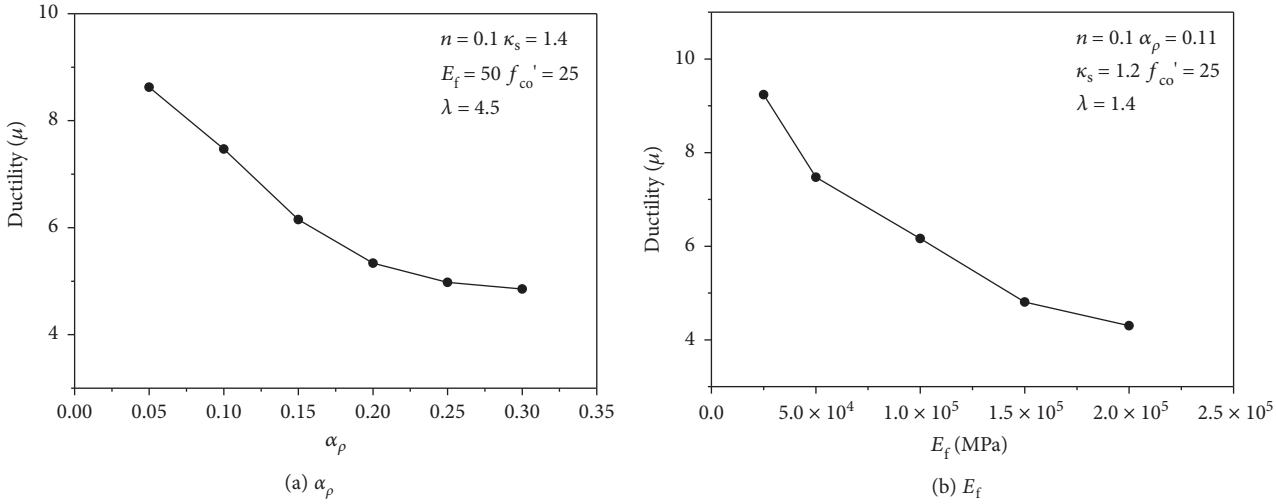

(a) α_ρ (b) E_f

Figure 11: Variation of ductility with different parameters.

3.3.2. Energy Dissipation. To evaluate the energy dissipation capacity of the strengthened columns, a cyclic loading analysis was conducted in OS with a similar loading pattern as in experiments for all specimens in analysis with different parameters. For each specimen, three major factors [3], including energy dissipation (E_h), elastic strain energy (E_e), and equivalent viscous damping ratio (ξ_{eq}), were calculated for each hysteric loop with MATLAB.

Among all parameters, the shear span ratio showed the most significant effect on energy dissipation capacity. Both of the energy dissipation and elastic strain energy decrease rapidly with the increase in shear span ratio, as shown in Figure 12(a), due to the stress level decrease in columns. In addition, the equivalent viscous damping ratio, which reflects the plastic strain energy, was relatively small for a column with a relatively big shear span ratio, which was due to the fact that the plastic strain energy was mainly contributed by concrete cracking, which would be relatively less to a column with a relatively big shear span ratio, especially when the drift ratio was relatively small. As shown in Figure 12(b), when the drift ratio equals to 0.01, the equivalent viscous damping ratio of the column (=0.048) when $\lambda = 8.85$ was only 32% that of the column (=0.148) when $\lambda = 3.18$, and this difference would gradually diminish with the increase in drift ratio. After the drift ratio reached 0.09, the development of the equivalent viscous damping ratio was almost coincident for all specimens with the increase in the drift ratio.

Due to the elastic property of FRP reinforcement, which contributes no energy dissipation to the column, the energy dissipation of columns with different EQFRR would remain constant, which has been proved in analysis, as shown in Figure 13(a); the energy dissipation curves with different EQFRR were basically coincident with each other. In addition, increasing EQFRR would downgrade the stress level of steel bars by "transforming" more stress from the steel bars to the FRP bars; the elastic strain energy of each cycle of

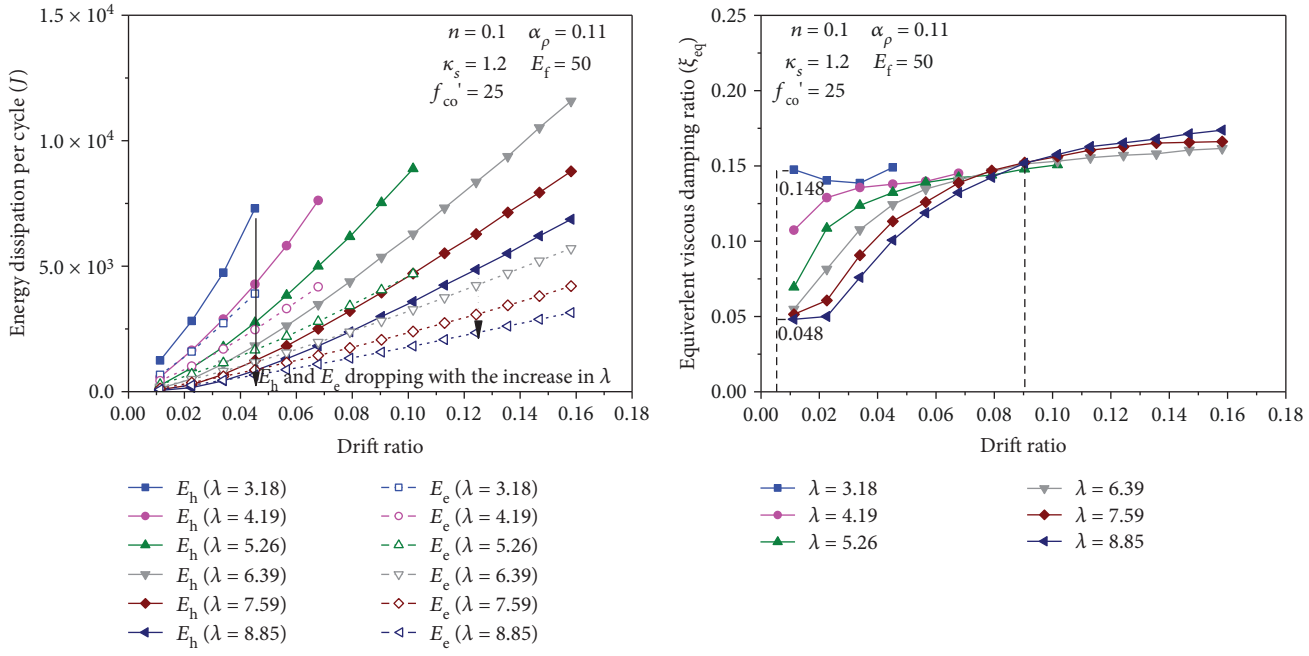

(a) Energy dissipation (b) Equivalent viscous damping ratio

Figure 12: Variation of energy dissipation indicators with drift ratio along with λ.

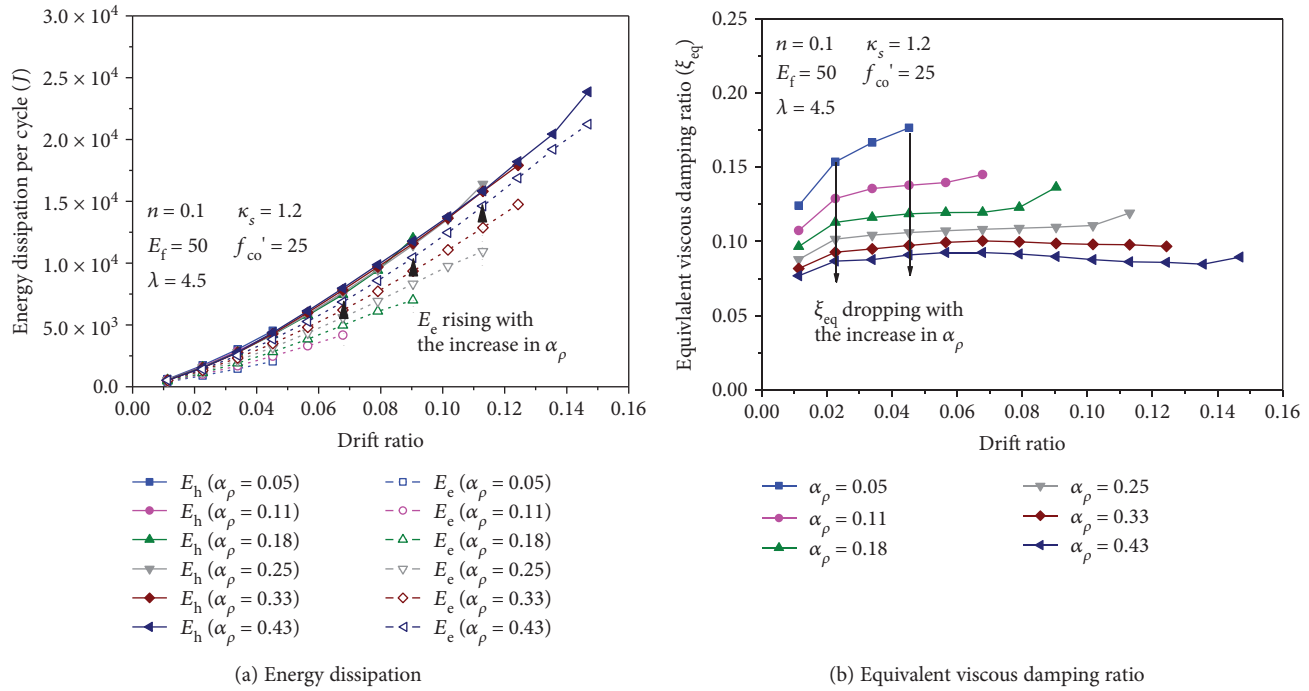

(a) Energy dissipation (b) Equivalent viscous damping ratio

Figure 13: Variation of energy dissipation indicators with drift ratio along with α_ρ.

hysteresis loops may increase with the increase in EQFRR under a certain drift ratio, which has also been proved in analysis. The elastic strain energy and equivalent viscous damping ratio, which refers to plastic strain energy, gradually increases and decreases with the increase in EQFRR, as shown in Figures 13(a) and 13(b), respectively. Moreover, the equivalent viscous damping ratio increased relatively slowly with the increase in drift ratio when a relatively high EQFRR was applied, as shown in Figure 13(b), which indicated that the increase in EQFRR could slow down the development of plastic strain energy in columns.

3.3.3. Lateral Stiffness. The lateral stiffness of the bridge column is a time-dependent property which may decrease in

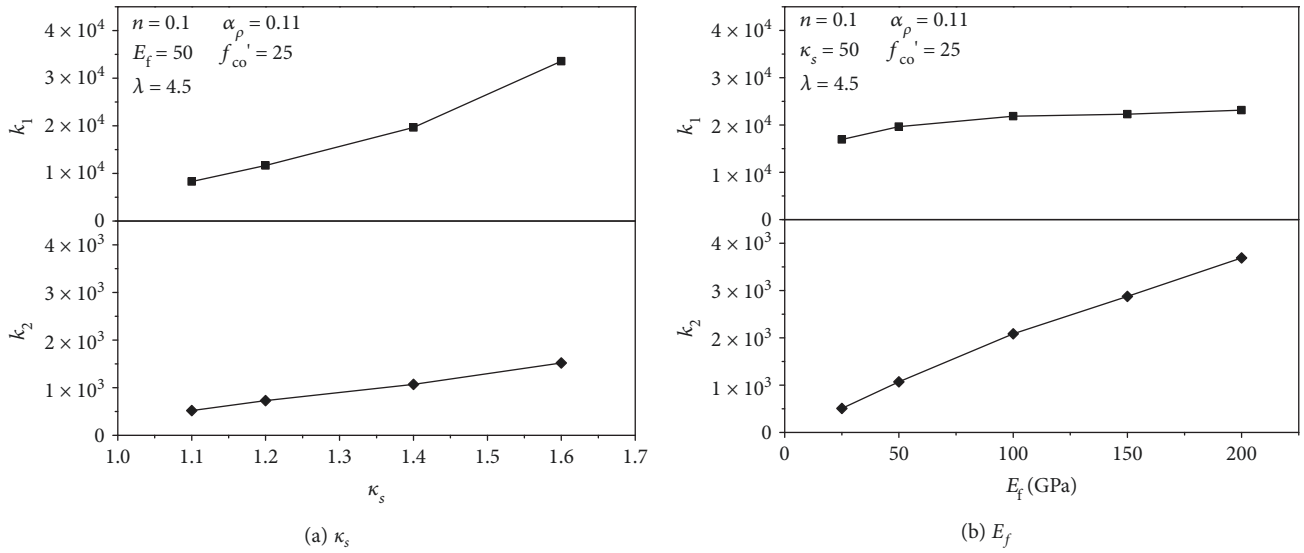

(a) κ_s (b) E_f

Figure 14: Variation of k_1 and k_2 with different parameters.

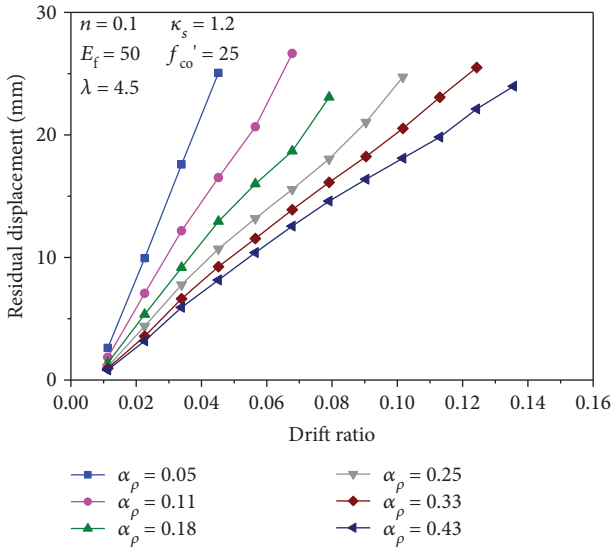

Figure 15: Variation of residual displacement with drift ratio along with α_ρ.

resistance of the gradually weakening anchoring condition affected especially by scouring along the structure's service life [28]. Therefore, extra stiffness demands should be considered in the strengthening process. Since the stiffness of the column is proportional to the flexural stiffness of the cross section (EI) and inversely proportional to the second power of the column height (h), the most effective way to enhance the stiffness is to change the dimensions of the column, such as enlarging the cross-sectional area or "shortening" the height of the column, which had been directly and indirectly considered in analysis through the expansion ratio and shear span ratio of the column, respectively. Take expansion ratio as an example; the initial stiffness (k_1) of the specimen increased by 300% with the expansion ratio increased by 45%, as shown in Figure 14(a), which suggested a high efficiency of expansion ratio on improving the initial stiffness. Other parameters, such as elastic modulus of FRP reinforcement, could also contribute to the initial stiffness yet not as remarkable as the expansion ratio and shear span ratio of the column, as shown in Figure 14(b).

A stable postyield stiffness stage was obtained by most specimens in the analysis. The column with a higher postyield stiffness generally represents less damage and better repairability when the earthquake strikes [29, 30], and the variation of postyield stiffness with different parameters was also evaluated in the analysis. Since the FRP reinforcement mainly contributes to the postyield stiffness of the column, the postyield stiffness increases rapidly and almost linearly with the increase in the elastic modulus of FRP reinforcement, as shown in Figure 14(b). Other parameters such as expansion ratio could also contribute to the postyield stiffness yet not as remarkable as the elastic modulus of FRP reinforcement, as shown in Figure 14(a).

3.3.4. Residual Displacement. The residual displacement is a critical parameter for evaluating the repairability of the structure after earthquakes [25], and it basically increases linearly with the drift ratio regardless of any parameters applied to the model, as shown in Figure 15. Residual displacement was mostly affected by EQFRR which showed a rapid decrease with the increase in EQFRR, as shown in Figure 15. This was due to the fact that the plastic deformation of the column developed rather slowly when a relatively high EQFRR was applied, which further indicated that a better repairability could be achieved with a relatively high EQFRR for the strengthened column.

4. Conclusions

A modeling method based on the fiber analysis concept was realized in OS, in which the cross-section model of the strengthened column was simplified based on different confinement conditions applied by a steel spiral stirrup and an FRP spiral stirrup, and the strain penetration of longitudinal

bars was also considered in the column model by using a zero-length-section element. A comprehensive parametric study was then further conducted to evaluate the influence of design parameters, such as axial load ratio, equivalent FRP reinforcement ratio rate (EQFRR), expansion ratio, elastic modulus of FRP reinforcement, compressive strength of concrete, and shear span ratio of the column, in terms of lateral load capacity, ductility, energy dissipation, lateral stiffness, and residual displacement of the strengthened column. The conclusions could be summarized as follows:

(1) The hysteric curves in the modeling were consistent with those in experiments. The yield load and peak load in modeling agree well with those in experiment with a maximal error of 3.6%. The postyield stiffness of hysteric curves is also closed to that of experimental hysteric curves with a maximal error of 11.1%. In addition, the residual displacement of each hysteric loop in modeling is basically consistent with that in the experiment, especially within the residual displacement limit, all of which indicates the high accuracy of the modeling method on predicting the seismic behavior of columns strengthened by the PPCP-FRP method.

(2) The lateral load capacity and ductility of strengthened columns were mostly affected by EQFRR. The yield load of strengthened columns increases with the increase in EQFRR due to the relatively high stress achieved by FRP bars when the strengthened column started yielding. The peak load of strengthened columns increases as well with the increase in EQFRR but due to the different fact that the column failure is characterized by the fracture of FRP bars; therefore, when a higher EQFRR was applied, the higher peak load would be obtained by strengthened columns. The ductility of the strengthened columns decreases with the increase in EQFRR due to the fact that the yield of the column was postponed with the increase in EQFRR.

(3) The shear span ratio of the column showed the most significant effect on the energy dissipation capacity of strengthened columns. With the increase in shear span ratio, both energy dissipation and elastic strain energy decrease rapidly due to the stress level decrease in columns. In addition, the equivalent viscous damping ratio, which reflects the plastic strain energy, was relatively small for a column with a relatively big shear span ratio, which was due to the fact that the plastic strain energy was mainly contributed by concrete cracking, which would be relatively less to a column with a relatively big shear span ratio, especially when the drift ratio was relatively small.

(4) The initial stiffness of strengthened columns was extremely sensitive to the expansion ratio, which increased by 300% with the expansion ratio increased by 45%. A stable postyield stiffness stage was obtained by most strengthened columns in a parametric study, and the value of postyield stiffness increases almost linearly and rapidly with the increase in elastic modulus of FRP reinforcement. The residual displacement of strengthened columns was mostly influenced by EQFRR, which rapidly decreases with the increase in EQFRR due to the fact that the plastic deformation of the column developed relatively slow when a relatively high EQFRR was applied, which further indicated that a better repairability could be achieved by applying a relatively high EQFRR in the strengthening process.

Data Availability

The datasets generated during the current study are available from the first author on reasonable request.

Conflicts of Interest

The authors declare that there are no conflicts of interest regarding the publication of this paper.

Acknowledgments

This research was financially supported by the National Key Research and Development Program of China (Grant no. 2016YFC0701100), the National Natural Science Foundation of China (Grant nos. 51525801 and 51778130), and the Fundamental Research Funds for the Central Universities (Grant no. 2242017k30002).

References

[1] J. Kattell and M. Eriksson, "Bridge scour evaluation: screening, analysis, & countermeasures," Tech. Rep. No. 9877 1207, SDTDC, 1998.

[2] P. F. Lagasse, *Countermeasures to Protect Bridge Piers from Scour*, Transportation Research Board, 2007.

[3] M. J. N. Priestley, F. Seible, and G. M. Calvi, *Seismic Design and Retrofit of Bridges*, John Wiley & Sons, 1996.

[4] B. J. Bett, R. E. Klingner, and J. O. Jirsa, "Lateral load response of strengthened and repaired reinforced concrete columns," *ACI Structural Journal*, vol. 85, no. 5, pp. 499–508, 1988.

[5] Y. H. Chai, M. N. Priestley, and F. Seible, "Seismic retrofit of circular bridge columns for enhanced flexural performance," *ACI Structural Journal*, vol. 88, no. 5, pp. 572–584, 1991.

[6] M. N. Priestley, F. Seible, Y. Xiao, and R. Verma, "Steel jacket retrofitting of reinforced concrete bridge columns for enhanced shear strength-part 1: theoretical considerations and test design," *ACI Structural Journal*, vol. 91, no. 4, pp. 394–405, 1994.

[7] A. Mirmiran and M. Shahawy, "Behavior of concrete columns confined by fiber composites," *Journal of Structural Engineering*, vol. 123, no. 5, pp. 583–590, 1997.

[8] Y.-L. Bai, J. G. Dai, and J. G. Teng, "Cyclic compressive behavior of concrete confined with large rupture strain FRP composites," *Journal of Composites for Construction*, vol. 18, no. 1, article 04013025, 2014.

[9] L.-Z. Yao and G. Wu, "Fiber-element modeling for seismic performance of square RC bridge columns retrofitted with

NSM BFRP bars and/or BFRP sheet confinement," *Journal of Composites for Construction*, vol. 20, no. 4, article 04016001, 2016.

[10] J.-G. Dai, L. Lam, and T. Ueda, "Seismic retrofit of square RC columns with polyethylene terephthalate (PET) fibre reinforced polymer composites," *Construction and Building Materials*, vol. 27, no. 1, pp. 206–217, 2012.

[11] T. C. Rousakis, "Reusable and recyclable nonbonded composite tapes and ropes for concrete columns confinement," *Composites Part B: Engineering*, vol. 103, pp. 15–22, 2016.

[12] T. C. Rousakis, "Inherent seismic resilience of RC columns externally confined with nonbonded composite ropes," *Composites Part B: Engineering*, vol. 135, pp. 142–148, 2018.

[13] H. Saadatmanesh, M. R. Ehsani, and L. Jin, "Repair of earthquake-damaged RC columns with FRP wraps," *ACI Structural Journal*, vol. 94, pp. 206–215, 1997.

[14] M. S. Saiidi and Z. Cheng, "Effectiveness of composites in earthquake damage repair of reinforced concrete flared columns," *Journal of Composites for Construction*, vol. 8, no. 4, pp. 306–314, 2004.

[15] A. Vosooghi and M. S. Saiidi, "Design guidelines for rapid repair of earthquake-damaged circular RC bridge columns using CFRP," *Journal of Bridge Engineering*, vol. 18, no. 9, pp. 827–836, 2013.

[16] A. Vosooghi and M. S. Saiidi, "Shake-table studies of repaired reinforced concrete bridge columns using carbon fiber-reinforced polymer fabrics," *ACI Structural Journal*, vol. 110, no. 1, p. 105, 2013.

[17] M. Fakharifar, G. Chen, C. Wu, A. Shamsabadi, M. A. ElGawady, and A. Dalvand, "Rapid repair of earthquake-damaged RC columns with prestressed steel jackets," *Journal of Bridge Engineering*, vol. 21, no. 4, article 04015075, 2016.

[18] J. Li, J. Gong, and L. Wang, "Seismic behavior of corrosion-damaged reinforced concrete columns strengthened using combined carbon fiber-reinforced polymer and steel jacket," *Construction and Building Materials*, vol. 23, no. 7, pp. 2653–2663, 2009.

[19] S. Mazzoni, F. Mckenne, M. Scott, and G. L. Fenves, *Open System for Earthquake Engineering Simulation User Manual, Version 2.0*, University of California, Pacific Earthquake Engineering Center, Berkeley, CA, USA, 2009.

[20] N. G. Bunni, B. Scott, R. Park, and M. Priestley, "Stress-strain behavior of concrete confined by overlapping hoops at low and high-strain rates," *Journal of the American Concrete Institute*, vol. 79, no. 6, pp. 496–498, 1982.

[21] G. Wu, Z. T. Lü, and Z. S. Wu, "Strength and ductility of concrete cylinders confined with FRP composites," *Construction and Building Materials*, vol. 20, no. 3, pp. 134–148, 2006.

[22] T. C. Rousakis and I. S. Tourtouras, "Modeling of passive and active external confinement of RC columns with elastic material," *ZAMM - Journal of Applied Mathematics and Mechanics/ Zeitschrift für Angewandte Mathematik und Mechanik*, vol. 95, no. 10, pp. 1046–1057, 2015.

[23] J. Teng, J.-F. Chen, S. T. Smith, and L. Lam, *FRP: Strengthened RC Structures*, Wiley, 2002.

[24] D. H. Deitz, I. E. Harik, and H. Gesund, "Physical properties of glass fiber reinforced polymer rebars in compression," *Journal of Composites for Construction*, vol. 7, no. 4, pp. 363–366, 2003.

[25] Committee J E E, *Earthquake Resistant Design Codes in Japan*, Japan Society of Civil Engineers (JSCE), 2000.

[26] L. Aashto, *Bridge Design Specifications*, American Association of State Highway and Transportation Officials, Washington, DC, USA, 1998.

[27] R. Park and T. Paulay, *Reinforced Concrete Structures*, John Wiley & Sons, 1975.

[28] A. Fioklou and A. Alipour, "Seismic behavior of bridges with deep foundations under effects of scouring," in *Structures Congress 2014*, pp. 313–323, Boston, MA, USA, 2014, ASCE.

[29] Z.-Y. Sun, G. Wu, Z.-S. Wu, and M. Zhang, "Seismic behavior of concrete columns reinforced by steel-FRP composite bars," *Journal of Composites for Construction*, vol. 15, no. 5, pp. 696–706, 2011.

[30] M. F. M. Fahmy, Z. Wu, G. Wu, and Z. Sun, "Post-yield stiffnesses and residual deformations of RC bridge columns reinforced with ordinary rebars and steel fiber composite bars," *Engineering Structures*, vol. 32, no. 9, pp. 2969–2983, 2010.